Article

Phytoestrogen *β*-Sitosterol Exhibits Potent In Vitro Antiviral Activity against Influenza A Viruses

Sara Shokry [1,2], Akram Hegazy [3], Ahmad M. Abbas [2,4], Islam Mostafa [5], Ibrahim H. Eissa [6], Ahmed M. Metwaly [7,8], Galal Yahya [9], Assem M. El-Shazly [5,10], Khaled M. Aboshanab [2,*] and Ahmed Mostafa [1,*]

1. Center of Scientific Excellence for Influenza Viruses, National Research Centre, Giza 12622, Egypt
2. Department of Microbiology and Immunology, Faculty of Pharmacy, Ain Shams University, Abbassia, Cairo 11566, Egypt
3. Department of Agricultural Microbiology, Faculty of Agriculture, Cairo University, Giza District, Giza 12613, Egypt
4. Department of Microbiology and Immunology, Faculty of Pharmacy, King Salman International University (KSIU), Sinai 46612, Egypt
5. Department of Pharmacognosy, Faculty of Pharmacy, Zagazig University, Zagazig 44519, Egypt
6. Pharmaceutical Medicinal Chemistry & Drug Design Department, Faculty of Pharmacy (Boys), Al-Azhar University, Cairo 11884, Egypt
7. Pharmacognosy and Medicinal Plants Department, Faculty of Pharmacy (Boys), Al-Azhar University, Cairo 11884, Egypt
8. Biopharmaceutical Products Research Department, Genetic Engineering and Biotechnology Research Institute, City of Scientific Research and Technological Applications (SRTA-City), Alexandria 21934, Egypt
9. Department of Microbiology and Immunology, Faculty of Pharmacy, Zagazig University, Zagazig 44519, Egypt
10. Faculty of Pharmacy, El Saleheya El Gadida University, El Saleheya El Gadida 44813, Sharkia, Egypt
*   Correspondence: aboshanab2012@pharma.asu.edu.eg (K.M.A.); ahmed_elsayed@daad-alumni.de (A.M.)

Abstract: Influenza is a contagious infection in humans that is caused frequently by low pathogenic seasonal influenza viruses and occasionally by pathogenic avian influenza viruses (AIV) of H5, H7, and H9 subtypes. Recently, the clinical sector in poultry and humans has been confronted with many challenges, including the limited number of antiviral drugs and the rapid evolution of drug-resistant variants. Herein, the anti-influenza activities of various plant-derived phytochemicals were investigated against highly pathogenic avian influenza A/H5N1 virus (HPAIV H5N1) and seasonal low pathogenic human influenza A/H1N1 virus (LPHIV H1N1). Out of the 22 tested phytochemicals, the steroid compounds *β*-sitosterol and *β*-sitosterol-*O*-glucoside have very potent activity against the predefined influenza A viruses (IAV). Both steroids could induce such activity by affecting multiple stages during IAV replication cycles, including viral adsorption and replication with a major and significant impact on the virus directly in a cell-free status "viricidal effect". On a molecular level, several molecular docking studies suggested that *β*-sitosterol and *β*-sitosterol-*O*-glucoside exhibited viricidal effects through blocking active binding sites of the hemagglutinin surface protein, as well as showing inhibitory effects against replication through the binding with influenza neuraminidase activity and blocking the active sites of the M2 proton channel activity. The phytoestrogen *β*-sitosterol has structural similarity with the active form of the female sex hormone estradiol, and this similarity is likely one of the molecular determinants that enables the phytoestrogen *β*-sitosterol and its derivative to control IAV infection in vitro. This promising anti-influenza activity of *β*-sitosterol and its *O*-glycoside derivative, according to both in vitro and cheminformatics studies, recommend both phytochemicals for further studies going through preclinical and clinical phases as efficient anti-influenza drug candidates.

Keywords: respiratory viruses; COVID-19; influenza; *β*-sitosterol; molecular docking (MD)

1. Introduction

Annual epidemics resulting from viral respiratory infections such as the common cold and influenza-like sicknesses lead to tragic impacts on global public health. They contribute substantially to high rates of morbidity and mortality worldwide [1]. The current COVID-19 pandemic serves as an example of how RNA viruses generate human, animal, and zoonotic infections that afflict millions of people. Viral respiratory infections are the utmost reason to seek health care in developing and developed countries [2,3]. Infections caused by respiratory viruses kill about 5 million children (<5 years) every year all over the world [4].

There is a huge number of respiratory viruses (>200 viruses) belonging to six families, namely *Adenoviridae*, *Herpesviridae*, *Picornaviridae*, *Orthomyxoviridae*, *Paramyxoviridae*, and *Coronaviridae* [5]. Nonetheless, family members of *Orthomyxoviridae* (especially influenza viruses) and *Coronaviridae* (especially severe acute respiratory syndrome coronavirus (SARS-CoV), Middle East respiratory syndrome (MERS), and SARS-CoV-2) have attracted more attention in the past two decades [6,7]. Seasonal outbreaks, endemic infections, and suddenly occurring pandemic situations are felt mainly within these two families [8–10]. All ages are susceptible to infection with influenza viruses and coronaviruses; however, young children (<5 years) and aged people (>65 years) have the highest incidence rate and may suffer more [11,12].

On a global scale, the reported number of severe cases caused only by influenza epidemics is about 3 to 5 million people, causing about 291,243 to 645,832 fatal cases. In the United States, cost-of-illness (COI) studies revealed an annual economic loss of about USD 87.1 billion [13,14]. Every 5 to 10 years, a new influenza pandemic event catches everyone off guard. It is mainly driven by the emergence of novel flu strains belonging to genus A of influenza viruses (IAV) [15]. Both influenza viruses and coronaviruses share the common features of being enveloped viruses with single-stranded RNA genomes. Unlike DNA viruses, RNA viruses are more prone to evolution, as they do not possess replication machinery with proofreading ability, which introduces continual changes to the viral genome, resulting in new strains [5,16].

A lack of immunity in individuals to a new viral strain(s) complicates infection control, ending with a global pandemic [17]. The postexposure use of antiviral drugs to cure respiratory viral infections is one of the successful chemoprophylaxis approaches [18]. Biologically active plant-metabolized products and plant extracts (e.g., flavonoids, terpenoids, steroids, polyphenols, saponins, coumarins, and lignans) are considered effective and safe therapeutic tools to combat respiratory viral infections [19–22]. The pharmacological pipeline for the prevention and treatment of prospective flu-like outbreaks will be widened by further investigation of these phytochemical medicines for clinical use [21]. In this study, different phytochemical classes were screened for their antiviral potential against avian and seasonal IAVs of subtypes H1N1 and H5N1 to find out safe, novel, and potent anti-influenza drug candidates. In addition, the stages of antiviral action of certain plant steroids (β-sitosterol and β-sitosterol-*O*-glucoside) that show promising anti-influenza activity have been investigated against the seasonal influenza A/H1N1 virus.

2. Materials and Methods

2.1. Cell Lines and Viruses

Madin Darby Canine Kidney (MDCK) cell line was obtained from the cell culture collection of the Center of Scientific Excellence for Influenza Viruses (CSEIV), National Research Centre (NRC), Cairo, Egypt, and were grown into monolayer culture using Dulbecco's modified Eagle's medium (DMEM) (DMEM; BioWhittaker, Walkersville, MD, USA) supplemented with 1% Penicillin/Streptomycin (pen/strep) antibiotic/antimycotic mixture (GIBCO-BRL; New York, NY, USA) and 5% fetal bovine serum (FBS) (Gibco-BRL; New York, USA). The cells were serially passaged and plated into 96-well, 12-well, and 6-well growth plates for cytotoxicity, plaque reduction, and mode of action, and proliferated at 37 °C in a humified environment with 5% CO_2 whenever the monolayers were con-

fluent. Consistently, two strains of IAVs, namely the highly pathogenic avian influenza A/chicken/Egypt/N12640A/2016 (H5N1) and seasonal influenza A/Egypt/NRC098/2019 (H1N1) (GISAID ID: EPI_ISL_12995118) provided by the CSEIV, NRC, Egypt, were routinely grown in MDCK cells and/or specific pathogen-free (SPF) embryonated chicken eggs (ECE) [23,24]. Supernatants of infected cells were used to create virus stock cultures, which were then stored at −80 °C for short-term use. The viruses were titrated using median tissue culture infectious dose (TCID50) assay and plaque infectivity assay (PIA) as previously described [20].

2.2. Phytochemicals

Silybin, 7-hydroxyflavone, flavanone, saponin, lupeol, gluconic acid, galacturonic acid, D-sorbitol, digitonin, arbutin, D- (-) salicin, kaempferitrin, isoquercitrin, chrysophanic acid, aloe-emodin, o-coumaric acid, and vanillin were purchased from Sigma, St. Louis, MO, USA. Pinocembrin, *β*-sitosterol, and *β*-sitosterol-*O*-glucoside were isolated from *Centaurea eryngioides* [25]. Glucuronic acid and ouabain were obtained from Serva, Feinbiochemica, Heidelberg, Germany. Naringin was isolated from the peel of *Citrus jambhiri* Lush. fruit [26]. The investigated phytochemicals in the current study are discussed in Table 1.

Table 1. The chemical classification and biological activities of the phytochemicals and drug control used in this study.

Compound	CAS No.	Class	Reported Biological Activities	Reference
Silybin	22888-70-6	Flavonoids	Anti-inflammatory and antiviral	[27,28]
7-Hydroxy flavone	6665-86-7	Flavonoids	Anti-inflammatory and antiviral	[29–31]
Pinocembrin	480-39-7	Flavonoids	Anti-inflammatory, antiallergic, antioxidant, anticarcinogenic, and antiviral	[32–35]
Flavanone	487-26-3	Flavonoids	Anti-inflammatory	[36]
Saponin	8047-15-2	Triterpene	Antimicrobial, anticancer, antioxidant, antitumor, and antiviral	[37–40]
Lupeol	545-47-1	Triterpene	Antioxidant and anti-inflammatory, Antiviral (Lupeol synthetic derivatives)	[41–43]
Glucuronic acid	528-16-5	Sugar acids	Antioxidant, hepatoprotective, and antiviral	[44,45]
Galacturonic acid	9046-38-2	Sugar acids	Antiviral (As a saponin component)	[45–48]
D-sorbitol	50-70-4	Sugar alcohol Carbohydrates	Antiviral and laxative.	[49,50]
β-sitosterol	83-46-5	Steroids	Antioxidant, anticarcinogenic, anti-inflammatory, and antiviral	[51–54]
β-sitosterol-*O*-glucoside	474-58-8	Steroids	Antidiabetic, anticancer and antiviral	[55–57]
Ouabain	630-60-4	Steroid cardiac glycosides	Anticancer and antiviral	[58–61]
Digitonin	11024-24-1	Steroid saponin glycosides	Lipid solubilizing and antiviral	[62–64]
Arbutin	497-76-7	Phenolic glycosides	Antimelanogenesis, antidiuretic, and antiviral	[65,66]
D- (-) salicin	138-52-3	Phenolic glycosides	Antiviral and anti-inflammatory.	[67–69]
Naringin	10236-47-2	Flavonoid glycosides	Anti-inflammatory, anticancer, and antiviral	[70–73]
Kaempferitrin	482-38-2	Flavonoid glycosides	Hypoglycemic, anti-inflammatory, and antiviral	[74–77]
Isoquercitrin	482-35-9	Flavonoid glycosides	Antioxidant, antipruritic, neuroprotective, antibacterial, hepatoprotective, anti-inflammatory, and antiviral	[78–82]

Table 1. *Cont.*

Compound	CAS No.	Class	Reported Biological Activities	Reference
Chrysophanic acid	481-74-3	Anthraquinones	Antiviral	[83,84]
Aloe emodin	481-72-1	Anthraquinones	Antiviral, anticancer, anti-inflammatory, and antibacterial.	[85–91]
O-Coumaric acid	614-60-8	Phenols	Antiadipogenesis, antioxidant, and antiviral (as a component of a plant, indirectly)	[92–95]
Vanillin	121-33-5	Phenols	Antiviral, antimicrobial, anti-inflammatory, antiapoptotic, neuroprotective, and antioxidant	[96–100]
Zanamivir	139110-80-8	NAIs	Anti-influenza	[101]

NAIs: neuraminidase inhibitors; CAS No.: Chemical Abstracts Service Registry Number.

2.3. Cytotoxicity and Antiviral Assay

Crystal violet assay, described earlier [102,103], was employed to determine the cytotoxic range of concentrations for each the tested compounds on the predefined cell lines through CC_{50} determination and to primarily investigate their antiviral potential against the IAVs and SARS CoV-2. Initially, 96-well cell culture plates were seeded with MDCK cells at cell density of 1×10^5 cells/mL and incubated overnight under humified conditions at 37 °C in 5% CO_2 atmosphere. Then, the cells were washed with 1x sterile DPBS and the compounds under investigation were serially added to the plates in tenfold dilution with triplicates while cell control wells were included. The plates were incubated in humified incubator at 37 °C with a 5% CO_2 atmosphere for 3 days. Following incubation period, the plates underwent cell fixation with paraformaldehyde (10%) and visualization of CPE was then employed using the crystal violet stain (0.1%). Following routine washing with water, as previously mentioned, the plates were then left to dry overnight at 25 °C (room temperature). A volume of 100 µL of methanol (99.85%) was added over the stained cells to dissolve the crystal violet stain and to produce an optical density (OD), which was then measured using Anthos Zenyth 200rt reader (Anthos Labtec Instruments, Heerhugowaard, Netherlands) at a wavelength of 570 nm. In the same context, to assess the antiviral potential of the tested compounds, IC_{50} values were determined for each compound. Likewise, the cell lines (MDCK and Vero cells) were propagated in 96-well cell culture plates with the same densities as mentioned before. Viral adsorption step was conducted for 1 h at RT after routinely washing the cultured cells with sterile 1x DPBS. Immediately, 100 µL/well of each safe concentration (non-cytotoxic) for each compound was added to the cells, where cell and virus control wells were included, then the plates underwent a longer incubation time at 37 °C with 5% CO_2 conditions in a humified incubator for 3 days. The plates then went through the same procedures of fixation, visualization, and OD measurement as in CC_{50} determination protocol.

2.4. Plaque Reduction Assay (PRA)

To ascertain the antiviral potential of the highly promising steroid compounds, the plaque reduction assay [103] was carried out with minor changes. In brief, viral dilutions were added to a range of nontoxic concentrations for each compound and incubated at RT for 1h. The mixture was then added in triplicates to confluent monolayers of MDCK cells (80–90% confluency), previously proliferated 12-well cell culture plates for 24 h, and the plates were then incubated at 37 °C with CO_2 atmosphere to allow for viral adsorption onto host cell receptors. In the meantime, the plates were manually shaken smoothly at 15 min interval. Aspiration of residual inocula and washing with 1x sterile DPBS were then employed. Moreover, the plates were overlaid with 1% agarose and $1\times$ DMEM as $2\times$ overlay medium supplemented with 4 % BSA, 1% pen/strep mixture, and 1 µg/mL TPCK-treated trypsin (in case of working with H1N1 virus) and allowed to set. A longer incubation period for 60–72 h was carried out in humified incubator at 37 °C with 5% CO_2 atmosphere. The same procedures of cell fixation and plaque visualization were handled

as in plaque infectivity assay. The viral reduction percentage for each compound was then calculated according to the following equation [103]:

$$\text{Viral reduction } (\%) = \frac{\text{Count of untreated virus (control)} - \text{Count of treated virus}}{\text{Count of untreated virus (control)}} \times 100$$

2.5. Stage(s) of the Antiviral Action

The stages at which the steroids (β-sitosterol and β-sitosterol-*O*-glucoside) with promising anti-influenza activity have been investigated against the seasonal influenza A/H1N1 virus. The three investigated targets for the antiviral action(s) are (1) the viral adsorption onto the host-cell receptor preventing virus adhesion, (2) the viral replication inside the host cells, and (3) the targeting of the viral particles away from the cell (cell-free viricidal effect). The impact of the potent compound on each of the three predefined stages was investigated using modified protocols of plaque reduction assays as described previously [20].

2.6. Data Collection and Heatmap Construction

The data covering sex-disaggregated numbers of influenza deaths during 2015, 2018, and 2019 were retrieved from the EU's standardized death rate for diseases of respiratory system source Eurostat [104]. The heatmaps were created using the Clustvis online tool [105]; countries with constant numbers of both sexes were removed from the heatmap during the data processing.

2.7. In Silico Docking Studies

2.7.1. Protein Preparation

The crystal structures of influenza hemagglutinin H1 mutant DH1E (PDB ID: 5VMG, resolution: 2.45 Å), neuraminidases (PDB ID: 3TI5, resolution: 1.90 Å), proton channel M2 protein (PDB ID: 2RLF), and hemagglutinin head epitope of influenza H1N1 virus (PDB ID: 7MEM) were obtained from Protein Data Bank (https://www.rcsb.org) (accessed on 10 December 2022). At first, the crystal structures of the selected proteins were prepared by removing crystallographic water molecules. Only one chain for each protein was retained besides the cocrystallized ligands. For influenza M2 proton channel protein, we used all chains in the docking process. Protein chains were protonated using the following setting. The used electrostatic functional form was GB/VI with a distance cut-off of 15 Å. The used value of the dielectric constant was 2 with an 80 dielectric constant of the used solvent. The used Van der Waals functional form was 800R3 with a distance cut-off of 10 Å. Then, minimization of energy was carried out. Next, the active pockets of different proteins were determined. The residues in the proteins that were within 5 Å of the cocrystallized ligand's edge were identified as the active sites [106].

2.7.2. Ligand Preparation

Structures of the tested compounds were drawn using ChemBioDraw Ultra 14.0 and saved in MDL-SD file format. These were protonated and optimized by energy minimization using MM2 force field [107].

2.7.3. Docking Setup and Validation of Docking Protocol

MOE version 2019 was used in the docking studies. To validate the docking procedure, redocking of the cocrystallized ligands was carried out against the different active sites. Then, the produced RMSD values were calculated. The value less than 2 Å indicates the validity of the docking processes [108].

The docking procedures were carried out against the active sites producing setup for the 30 docked poses for each ligand using ASE as a scoring function [109]. The pose with good binding mode was selected. Discovery Studio (DS) 4.0 was used for visualization step [110]. Comparing the binding mode of the tested compounds with that of the reference molecules gives good insight about the binding pattern of the tested compounds [111,112].

2.8. Statistical Analysis

Using GraphPad Prism software version 5.04 (GraphPad Software Inc., La Jolla, CA, USA), statistical analysis was conducted using two-tailed unpaired T-tests. A value of $p \leq 0.05$ was considered to indicate statistical significance.

3. Results

3.1. Cytotoxicity and Antiviral Potential of the Investigated Compounds

Different classes of phytochemical compounds were chosen based on their reported biological activities (Table 1), and a preliminary screening was carried out in order to evaluate their possible antiviral efficacy against the IAVs after assessing their toxic effects on the MDCK cells. The anti-influenza activities of the tested compounds were compared to the reference zanamivir drug that represents the main antiviral class against influenza, namely neuraminidase inhibitors (NAIs). Notably, almost all tested compounds showed reliable safe use on the tested cell line, with concentrations reaching up to 10 mg/mL for most of the compounds (Figure 1 and Supplementary Figure S1). The antiviral potential of these compounds was first evaluated against the seasonal human influenza A/H1N1 virus and compared with the predefined drug control.
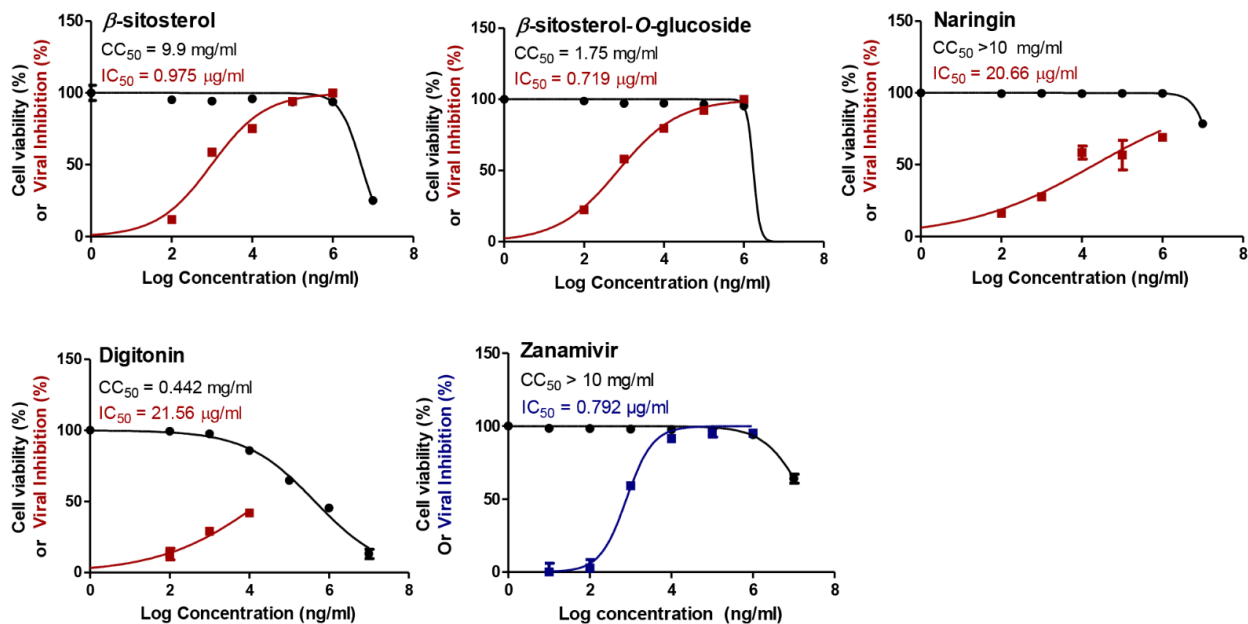

Figure 1. The cytotoxicity as expressed in CC_{50} (half-maximal cytotoxic concentration) and the antiviral efficacy against A/H1N1 as expressed in IC_{50} (half-maximal inhibitory concentration) for the studied phytochemicals. GraphPad Prism 5.01 software was used to analyze the nonlinear regression while the CC_{50} and IC_{50} were determined by plotting log inhibitor against normalized response (variable slope).

Strikingly, the steroid compounds β-sitosterol and β-sitosterol-*O*-glucoside clearly exerted highly promising antiviral activities against the tested A/H1N1 virus, with IC_{50} values of 0.975 and 0.719 μg/mL, respectively (Figure 1).

On the other hand, naringin, kaempferitrin, lupeol, and digitonin (Figure 1) moderately showed their antiviral potential against the tested IAV, with IC_{50} values equal to 20.66, 47.8, 93.68, and 21.56 μg/mL, respectively. Unfortunately, the rest of the compounds elucidated poor or no antiviral activities against the HPAIV (A/H5N1) when compared to the drug control (Figure S1). According to the SI values (Table 2), the highly efficacious steroids (β-sitosterol and β-sitosterol-*O*-glucoside) were assessed for their anti-influenza potential against the highly pathogenic avian influenza A/H5N1 virus, so as to depict their broad-spectrum use against different IAV subtypes.

Table 2. Selectivity indices for the screened compounds against influenza A/H1N1 and A/H5N1 subtypes.

Compound	Virus	CC_{50} (mg/mL)	IC_{50} (mg/mL)	SI
Silybin	H1N1	9.48	N/A	ND
	H5N1		N/A	ND
7-Hydroxy flavone	H1N1	5.83	0.360	16.194
	H5N1		N/A	ND
Naringin	H1N1	>10	0.0206	>485.43
	H5N1		N/A	ND
Pinocembrin	H1N1	>10	>10	>1
	H5N1		N/A	ND
Kaempferitrin	H1N1	>10	0.0478	>209.20
	H5N1		N/A	ND
Flavanone	H1N1	0.45	N/A	ND
	H5N1		N/A	ND
Isoquercitrin	H1N1	0.71	0.167	4.25
	H5N1		N/A	ND
Saponin	H1N1	>10	0.326	>30.674
	H5N1		N/A	ND
Lupeol	H1N1	0.56	0.0936	5.98
	H5N1		N/A	ND
D-Glucuronic acid	H1N1	10.26	N/A	ND
	H5N1		N/A	ND
D-Galacturonic acid	H1N1	9.61	N/A	ND
	H5N1		N/A	ND
β-sitosterol	H1N1	9.9	0.000975	10,154
	H5N1		0.000295	33,559
β-sitosterol-*O*-glucoside	H1N1	1.75	0.000719	2434
	H5N1		0.000613	2855
Ouabain	H1N1	0.176	N/A	ND
	H5N1		N/A	ND
Digitonin	H1N1	0.442	0.0215	20.56
	H5N1		N/A	ND
Chrysophanic acid	H1N1	0.0461	N/A	ND
	H5N1		N/A	ND
Aloe emodin	H1N1	2.28	0.729	3.127
	H5N1		N/A	ND
Arbutin	H1N1	>10	0.764	>13.09
	H5N1		N/A	ND
O-Coumaric acid	H1N1	9.172	NA	ND
	H5N1		N/A	ND
Vanillin	H1N1	0.242	N/A	ND
	H5N1		N/A	ND
D-sorbitol	H1N1	>10	3.11	>3.215
	H5N1		N/A	ND
D-(-) salicin	H1N1	>10	N/A	ND
	H5N1		N/A	ND
Zanamivir	H1N1	>10	0.000792	>12,626
	H5N1		0.000265	>37,736

CC_{50}: half-maximal cytotoxic concentration; IC_{50}: half-maximal inhibitory concentration; SI: selectivity index = CC_{50}/IC_{50}.

Remarkably, β-sitosterol and β-sitosterol-O-glucoside exhibited similar activities against the A/H5N1 virus with lower IC_{50} values of 0.295 and 0.613 µg/mL, respectively, when compared to the zanamivir as drug control (Figure 2).
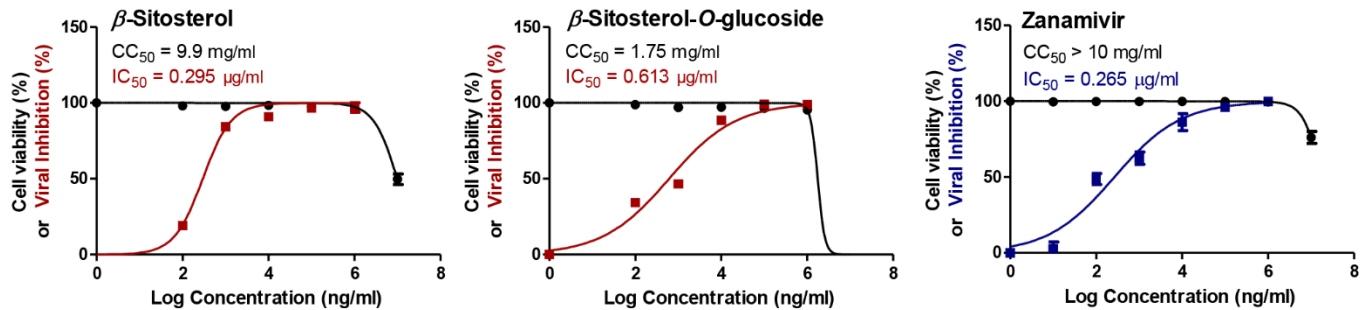

Figure 2. The cytotoxicity as expressed in CC_{50} (half-maximal cytotoxic concentration) and the antiviral potential against A/H5N1 as expressed in IC_{50} (half-maximal inhibitory concentration) for the most efficacious steroids (β-sitosterol and β-sitosterol-O-glucoside). GraphPad Prism 5.01 software was used to analyze the nonlinear regression, while the CC_{50} and IC_{50} were determined by plotting log inhibitor against normalized response (variable slope).

3.2. Viral titer Reduction in a Concentration-Dependent Manner

The plaque reduction assay was simply employed to validate the anti-IAV efficacy for the highly promising steroids β-sitosterol and β-sitosterol-O-glucoside (Figure 3a), based on their extremely high SI values as compared to the reference drug. Strikingly, the plaque reduction percentages clearly elucidated the anti-IAV potential against both influenza subtypes (H1N1 and H5N1) for both compounds where the viral titers had been lowered using low non-cytotoxic concentrations from the tested steroids (Figure 3b). These data support the hypothesis that the investigated steroids are considered as lead compounds to target influenza disease in both human and avian hosts.
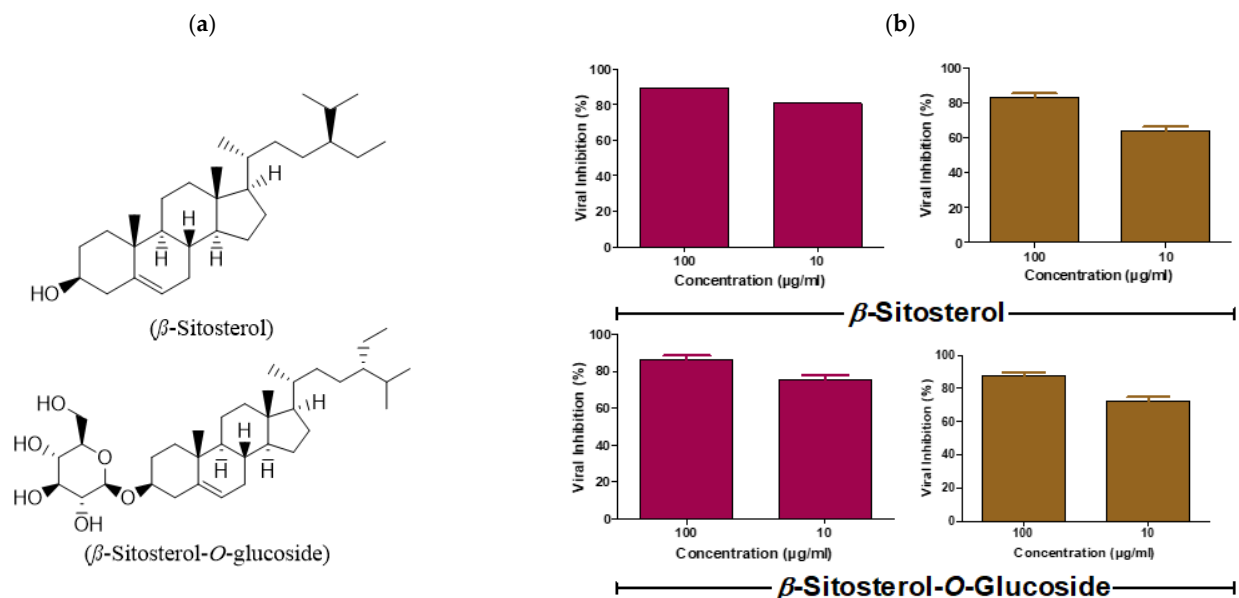

Figure 3. Concentration-dependent viral titer reduction for the highly promising steroids (β-sitosterol and β-sitosterol-O-glucoside) as determined via PRA. (**a**) Chemical structure of β-sitosterol and β-sitosterol-O-glucoside; (**b**) Validation of the anti-influenza efficacy for both compounds were evaluated against the A/H1N1 (dark pink) and the A/H5N1 (light brown), and GraphPad Prims 5.01 software was used to plot the viral inhibition percentages against compound concentrations.

3.3. β-Sitosterol and β-Sitosterol-O-Glucoside affects IAV at Multiple Stages of the Virus Replication Cycle

Noticeably, any antiviral compound works against the virus through three major specific mechanisms as previously described. In this context, we aimed to explore at which step in the influenza virus replication cycle the highly effective β-sitosterol and β-sitosterol-*O*-glucoside lowered the titer of A/H1N1 virus. Curiously, both compounds exhibited their anti-influenza potency through viricidal actions where they directly target the human seasonal influenza viral particles away from the host MDCK cells (Table 3).

Table 3. The mechanism of action(s) for the highly effective steroids as depicted through plaque reduction % in a concentration-dependent manner.

Steroid	Concentration (μg/mL)	Stage of Antiviral Action		
		Viral Replication	Viricidal	Viral Adsorption
β-sitosterol	1	31.8%	84%	28%
	10	41.2%	98.5%	37.5%
	100	52.9%	99%	52.5%
β-sitosterol-*O*-glucoside	1	28.7%	83.6%	35.8%
	10	37.7%	93.3%	48.3%
	100	52.8%	97.1%	56.9%

3.4. Docking studies

To understand the obtained antiviral activities at a molecular level, β-sitosterol and β-sitosterol-*O*-glucoside were docked against different viral protein targets. These proteins are influenza hemagglutinin H1 mutant DH1E (PDB ID: 5VMG, resolution: 2.45 Å), neuraminidase from influenza A/H1N1 virus (PDB ID: 3TI5, resolution: 1.90 Å), influenza proton channel M2 protein (PDB ID: 2RLF), and hemagglutinin head epitope of influenza H1N1 virus (PDB ID: 7MEM). 6′-Sialyl-*N*-acetyllactosamine, zanamivir, and rimantadine were used as reference molecules against hemagglutinin, neuraminidase, and M2 proteins, respectively. In the docking studies, it depended on both binding mode and binding energy to investigate the efficiency of binding against the active sites (Table 4).

Table 4. Binding free energies (ΔG in Kcal/mol) of β-sitosterol, and β-sitosterol-*O*-glucoside, against hemagglutinin, neuraminidase, M2, and hemagglutinin head epitope proteins as compared to the reference molecules.

Compound	Hemagglutinin	Neuraminidase	M2	Hemagglutinin Head Epitope
β-sitosterol	−6.40	−29.40	−10.97	−10.90
β-sitosterol-*O*-glucoside	−6.78	−30.13	−10.75	−8.97
6′-Sialyl-*N*-acetyllactosamine	−5.66	-	-	-
Zanamivir	-	−19.28	-	-
Rimantadine	-	-	−9.968	-

3.4.1. Validation

To validate the docking process, docking procedures were performed for the cocrystallized ligands in the active sites of influenza hemagglutinin H1 mutant DH1E, influenza A/H1N1 neuraminidase, and proton channel M2 utilizing MMFF94X as a force field and ASE as a scoring function allowed for the protocol's validation. The small RMSD values

between the docked poses and the cocrystallized ligands during the validation step indicated the feasibility of the used methodology for the intended docking experiments (1.14, 0.95, and 1.4 Å for influenza hemagglutinin H1 mutant DH1E, influenza A/H1N1 neuraminidase, and proton channel M2, respectively) (Figure 4).
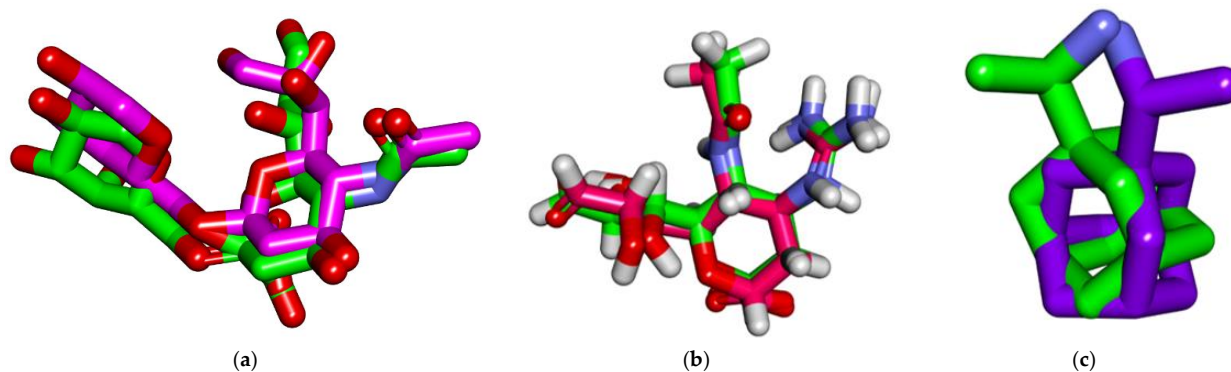

(**a**) (**b**) (**c**)

Figure 4. (**a**) Superimposition of the cocrystallized ligand (6′-sialyl-*N*-acetyllactosamine) of influenza hemagglutinin H1 mutant DH1E (carbon atoms in green) and the docked pose of the same ligand (carbon atoms in pink). (**b**) Superimposition of the cocrystallized ligand (zanamivir) of influenza A/H1N1 neuraminidase (carbon atoms in green) and the docked pose of the same ligand (carbon atoms in red). (**c**) Superimposition of the cocrystallized ligand (Rimantadine) of influenza proton channel M2 (carbon atoms in green) and the docked pose of the same ligand (carbon atoms in violet).

3.4.2. Docking Studies against Influenza Hemagglutinin H1 Mutant DH1E

The reference molecule (6′-Sialyl-*N*-acetyllactosamine) showed a binding score of -5.66 kcal/mol against influenza hemagglutinin H1 mutant DH1E. The *N*-((2S,3R,4R,5S,6R)-2,4,5-trihydroxy-6-(hydroxymethyl)tetrahydro-2*H*-pyran-3-yl)acetamide moiety was oriented into the first pocket of the active site, forming three hydrogen bonds with Lys218, Glu186, and Ser224. In addition, the (2R,3R,4S,5S,6R)-6-methyltetrahydro-2H-pyran-2,3, 4,5-tetraol moiety was oriented into the second pocket, forming two hydrogen bonds with Glu186 and Ser224. Furthermore, the (2S,4S,5R,6R)-5-acetamido-4-hydroxy-2-methoxy-6-((1S,2R)-1,2,3-trihydroxypropyl)tetrahydro-2*H*-pyran-2-carboxylic acid moiety occupied the third pocket, in close contact with Leu190, Val131, Thr129, Gly130, Thr151, and Glu127 (Figure 5A, Supplementary Figure S2).

Regarding the *β*-sitosterol, it exhibited a binding affinity of −6.40 Kcal/mol against influenza hemagglutinin H1 mutant DH1E. The hydroxyl group formed a hydrogen bond with Lys218. Steroid moiety formed two hydrophobic interactions with Leu222. The side chain ((*S*)-3-ethyl-2-methylheptane) formed three hydrophobic interactions with Trp149 and Leu190 (Figure 5B, Supplementary Figure S3).

Concerning *β*-sitosterol-*O*-glucoside, it showed a binding score of −6.78 Kcal/mol against influenza hemagglutinin H1 mutant DH1E. The sugar moiety formed four hydrogen bonds with Lys218, Glu186, and Ser224. The steroid moiety and the aliphatic side chain formed a close contact with Thr132, Val131, Thr129, Glu127, Gly154, Gly130, Trp149, Leu222 (Figure 5C, Supplementary Figure S4).
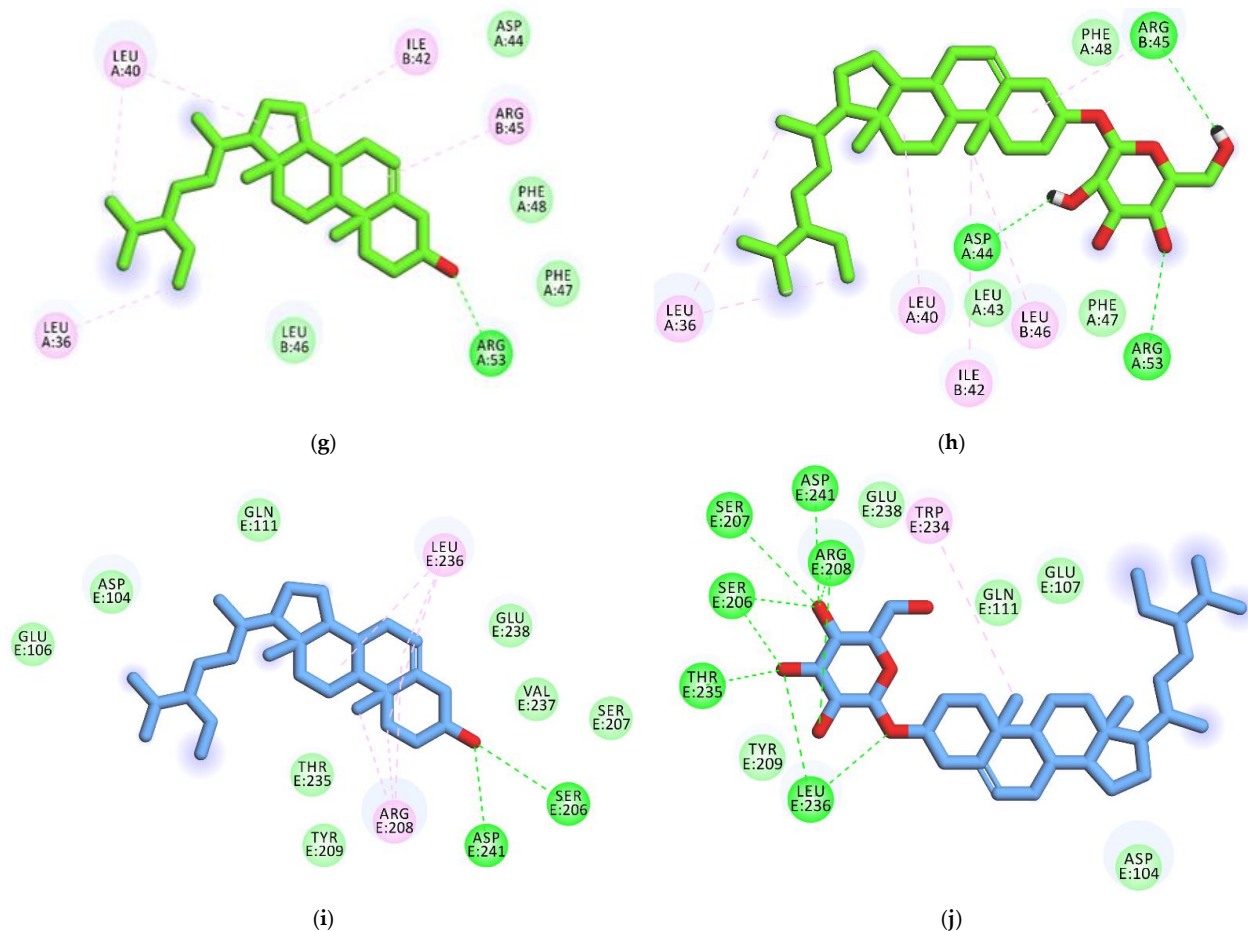
(a)

(b)

(c)

(d)

(e)

(f)

Figure 5. *Cont.*

(**g**)   (**h**)

(**i**)   (**j**)

Figure 5. (**a**) Two-dimensional image of 6′-Sialyl-*N*-acetyllactosamine docked into the active site of influenza A/H1N1 hemagglutinin; (**b**) 2D of β-sitosterol docked into the active site of influenza A/H1N1 hemagglutinin; (**c**) 2D of β-sitosterol-O-glucoside docked into the active site of influenza A/H1N1 hemagglutinin; (**d**) 2D of the cocrystallized ligand (Zanamivir) docked into the active site of influenza A/H1N1 neuraminidase; (**e**) 2D of β-Sitosterol docked into the active site of influenza A/H1N1 neuraminidase; (**f**) 2D of the cocrystallized ligand (Rimantadine) docked into the active site of influenza proton channel M2 protein; (**g**) 2D of β-sitosterol docked into the active site of influenza proton channel M2 protein; (**h**) 2D of β-sitosterol-o-glucoside docked into the active site of influenza proton channel M2 protein; (**i**) 2D of β-sitosterol docked into hemagglutinin head epitope; (**j**) 2D of β-sitosterol-o-glucoside docked into hemagglutinin head epitope.

3.4.3. Docking Studies against Influenza A/H1N1 Neuraminidase

The cocrystallized ligand (zanamivir) showed a binding sore of −19.28 kcal/mol against influenza A/H1N1 neuraminidase. The guanidine and acetamide moieties were oriented into the first pocket of the active site, forming six hydrogen bonds with Glu277, Trp178, Glu227, Arg152, and Asp151. The cyclohex-1-ene-1-carboxylic acid moiety was oriented into the second pocket, forming three hydrogen bonds with Arg371, Arg292, and Arg118. Furthermore, the propane-1,2,3-triol moiety occupied the third pocket, forming three hydrogen bonds with Glu276, Arg152, and Asn347 (Figure 5D, Supplementary Figure S5).

The results of docking studies revealed the correct binding mode of *β*-sitosterol against the active site of influenza A/H1N1 neuraminidase. In detail, *β*-sitosterol exhibited a binding affinity of −29.4003506 Kcal/mol against influenza A/H1N1 neuraminidase. The hydroxyl group formed a hydrogen bond with Arg430. The side chain ((S)-3-ethyl-2-methylh eptane) formed three hydrophobic interactions with Arg152, Arg224, and Ile222 (Figure 5E, Supplementary Figure S6).

3.4.4. Docking Studies against Influenza Proton Channel M2

The cocrystallized ligand (Rimantadine) showed a binding sore of -9.96808243 kcal/mol against influenza proton channel M2 protein. The ethanamine moiety was oriented into the deep pocket of the receptor, forming two hydrogen bonds with Asp44. The adamantane moiety was oriented into the outer region of the active site, forming three hydrophobic interactions with Leu46 and Leu40 (Figure 5F, Supplementary Figure S7).

In respect of β-sitosterol, it exhibited a binding affinity of -10.97 Kcal/mol against influenza proton channel M2 protein. The hydroxyl group formed a hydrogen bond with Arg430. The side chain ((S)-3-ethyl-2-methylheptane) formed three hydrophobic interactions with Arg152, Arg224, and Ile222 (Figure 5G, Supplementary Figure S8).

Respecting β-sitosterol-*O*-glucoside, it showed a binding score of -10.75 Kcal/mol against influenza M2 protein. The sugar moiety formed three hydrogen bonds with Arg45, Arg53, and Asp44. The steroid moiety and the aliphatic side chain formed six hydrophobic interactions with Arg45, Leu46, Ile42, Leu40, and Leu36 (Figure 5H, Supplementary Figure S9).

3.4.5. Docking Studies against Hemagglutinin Head Epitope of Influenza A/H1N1 Virus

The docking of both β-sitosterol and β-sitosterol-*O*-glucoside against hemagglutinin head epitope of influenza A/H1N1 virus revealed that β-sitosterol (binding score = -10.90) has a better binding mode and binding energy than β-sitosterol-*O*-glucoside (binding score = -8.97).

For β-sitosterol, it was completely buried inside the hemagglutinin head epitope. It formed two hydrogen bonds with Ser206 and Asp241. In addition, the steroid moiety formed six hydrophobic interactions with Leu236 and Arg208 (Figure 5I, Supplementary Figure S10).

Regarding β-sitosterol-*O*-glucoside, it exhibited a shallow binding with hemagglutinin head epitope. Only the sugar moiety was oriented into the pocket of hemagglutinin head epitope, forming nine hydrogen bonds with Arg208, Asp241, Ser207, Ser206, Thr235, and Leu236 (Figure 5J, Supplementary Figure S11). It can be concluded that β-sitosterol has a good chance to bind and block the hemagglutinin head epitope of the influenza A/H1N1 virus.

3.5. *Phytoestrogen β-Sitosterol Is Likely to Hinder IAV Replication in an Estrogen-Like Mode*

Recent studies discussing the existence of male-biased mortality in sex-disaggregated data of COVID-19 suggest that the female sex hormone estrogen is likely to contribute to this phenomenon [113]. Interestingly, by analyzing the sex-disaggregated datasets covering influenza deaths during 2015, 2018, and 2019 in 32 European countries with available indexed data according to the EU's standardized death rate for pulmonary diseases (Figure 6a,c,e), it was remarkable that the standardized death rates of males by influenza illness were higher during 2015 and 2018, but not significant compared to females for the same years. The mean death rates for males during 2015 and 2018 were 1.5 ± 0.1932 (mean $\pm$ SEM), and 3.7 ± 0.537, respectively, and the influenza death rates for females were 1.1 ± 0.1755 and 2.6 ± 0.4021 during 2015 and 2018, respectively (Figure 6b,d). The male death rates of influenza during 2019 were 1.72 higher than females, with mean values of 3.1 ± 0.3304 for males and 1.8 ± 0.1813 for females, demonstrating a significant difference between sexes and substantially biased mortality towards males (Figure 6f).

The phytoestrogen β-sitosterol and its derivative β-sitosterol-*O*-glucoside are structurally similar to estradiol, which is an estrogen steroid hormone and the major female sex hormone. The structural similarity between β-sitosterol and estradiol (Figures 3a and 7a) and the observed male-biased mortality in sex-disaggregated data of influenza deaths (Figure 6a–f) recommended the testing of the anti-influenza activity of estradiol. Interestingly, estradiol has high safety at a wide range of concentrations ($CC_{50} > 5$ mg/mL), with robust antiviral activity against seasonal influenza A/H1N1 virus ($IC_{50} = 7.1$ µg/mL)

(Figure 7b). Conclusively, estradiol showed antiviral activity against the influenza A/H1N1 virus in vitro but with a lower IC_{50} value, when compared with β-sitosterol.
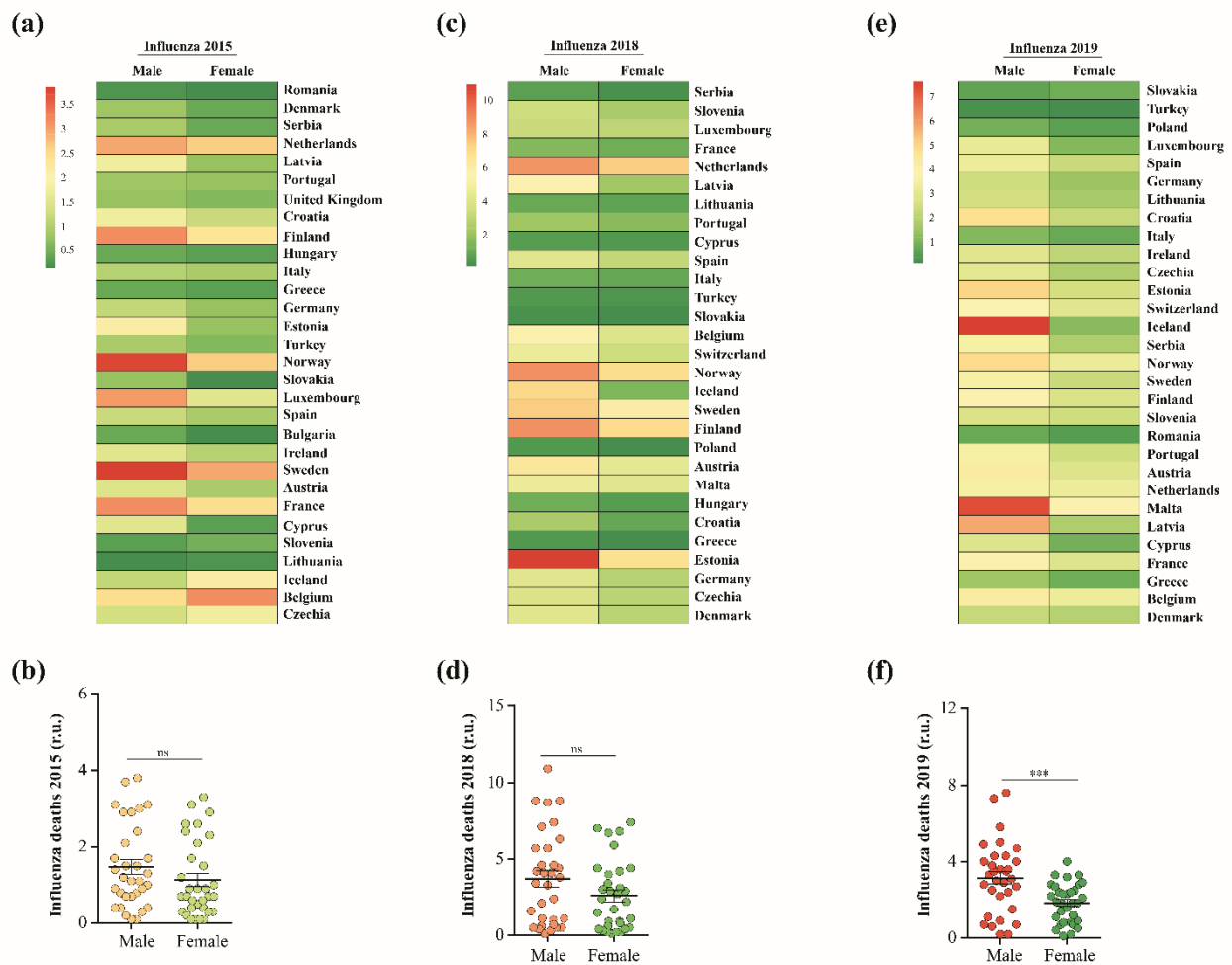

Figure 6. Sex-disaggregated data for influenza deaths during 2015, 2018, and 2019: (**a**) heatmap depicting sex differences in the death rates of influenza during 2015 in 30 EU countries; (**b**) mean differences between datasets representing both sexes in a; (**c**) heatmap depicting sex differences in the death rates of influenza during 2018 in 29 EU countries; (**d**) mean differences between datasets representing both sexes in c; (**e**) heatmap depicting sex differences in the death rates of influenza during 2019 in 30 EU countries; (**f**) mean differences between datasets representing both sexes in e. Results (**b,d,f**) are expressed as mean $\pm$ SEM. ns denotes no significance and *** $p \leq 0.001$.
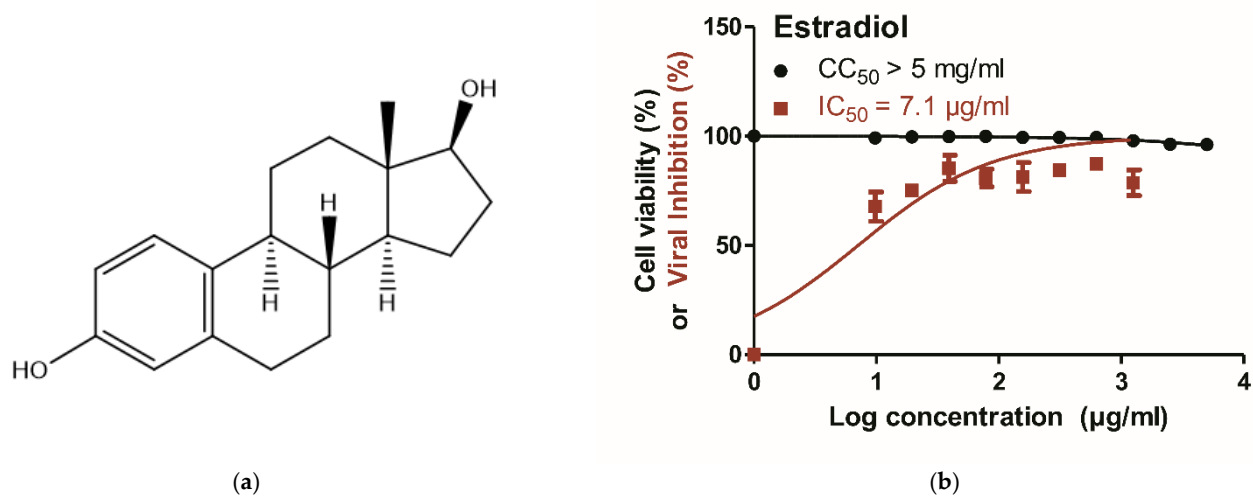
Figure 7. Structural similarity of β-sitosterol with estradiol and potential anti-influenza activity. (**a**) Chemical structure of the potent human estrogen form; namely estradiol; (**b**) the cytotoxicity of estradiol as expressed in CC_{50} and the antiviral activity against A/H1N1 as expressed as an IC_{50} value. GraphPad Prism 5.01 software was used to analyze the nonlinear regression, while the CC_{50} and IC_{50} were determined by plotting log inhibitor against normalized response (variable slope).

4. Discussion

The COVID-19 pandemic has highlighted the need for novel and safe antivirals that can combat emerging and reemerging respiratory RNA viruses [114]. Traditional medicine, which is ultimately based on plants and their secondary metabolites (i.e., phytochemicals), is considered one of the main therapeutic approaches to cure different diseases such as viral diseases, cancer, and chronic diseases (e.g., diabetes and heart diseases) [115]. In the last two decades, about 34% of the total newly approved drugs were naturally derived chemical substances [116]. Accordingly, we aimed at repurposing naturally occurring chemical compounds with different chemical classes as new antiviral candidates to help in controlling the respiratory viral infections, specifically avian and human IAVs.

Herein, we successfully unmasked the high antiviral potential of a well-known phytosterol, namely β-sitosterol and its *O*-glycoside derivative, against seasonal human influenza and avian viruses (H1N1 and H5N1 subtypes) with high SI values as compared to the standard FDA-approved anti-influenza drug (zanamivir). Additionally, the results revealed that low concentrations of this steroid compound (10–100 μg/mL) could inactivate up to 90% of viral infectivity through direct viricidal action on the A/H1N1 subtype.

A recent in silico study suggested that β-sitosterol could suppress viral infection with SARS-CoV-2 through targeting the receptor-binding domain (RBD) of the spike glycoprotein [54]. Previous investigations have shown also that β-sitosterol exhibits antioxidant, anti-inflammatory, anticancer, and in vitro antiviral activity against white spot syndrome virus [51–54]. However, antiviral activities against IAVs, to the best of our knowledge, have not yet been reported.

In addition to β-sitosterol, our results also showed robust antiviral activities of β-sitosterol-*O*-glucoside (Sitogluside or Daucosterol) against both tested IAVs, mainly via direct viricidal action. In addition, β-sitosterol-*O*-glucoside could induce up to 90% viral inhibition with very low concentration (10–100 μg/mL). The reported biological activities for β-sitosterol-*O*-glucoside have shown that it possesses anticancer and antidiabetic activities [55,57]. An in silico study for the antiviral effects of β-sitosterol-*O*-glucoside against SARS-CoV-2 have shown that sitogluside possesses inhibitory effects against the tested virus, as demonstrated by virtual study that revealed the capability of this compound to target the surface RBD of spike glycoprotein on the viral particle [56]. This emphasizes the observed viricidal mode of antiviral action of the investigated phytosterols against IAVs.

On the same hand, naringin proved to exhibit antiviral potential against human immunodeficiency virus type 1 (HIV-1), and an in silico study showed its potential to work against SARS-CoV-2, as it has high binding affinity to the virus's main protease [70,72]. Herein, naringin showed moderate antiviral activity against the influenza A/H1N1 virus, indicating its antiviral activity but to certain extent. Likewise, Gao and his colleagues have recently showed that digitonin has antiviral activity against Zika virus with low IC_{50} of 7.91 μM [117]; however, in this study, we showed that the digitonin has moderate antiviral activity against influenza A/H1N1 virus.

On the other hand, previous investigations on silybin using MTT assay to estimate the cytotoxicity and the SRB method to evaluate its antiviral assay (against A/ShanTou/169/06 (H1N1)) showed that silybin has high very low cytotoxicity on MDCK cells with a CC_{50} > 400 μM and low antiviral activity, with an EC_{50} value of 70.78±8.11 μM [28].. Our findings also proved the nontoxic effects of silybin on MDCK cells (CC_{50} value of 9.48 mg/mL) and poor anti-influenza potential against the human influenza A/H1N1 virus. However, 7-hydroxy flavanone showed antiviral activity against enterovirus type A-71 (EV-A71) [31], but it showed poor antiviral activity against A/H1N1 in this study. Likewise, previous reports proved the antiviral properties of pinocembrin against different viruses, including SARS-CoV-2, Zika virus (ZIKV), Herpesvirus type-1 (HSV-1), and Canine distemper virus [32,33,35], whereas in our findings, pinocembrin showed poor anti-H1N1 activity. Recently, a molecular docking (MD) simulation study also showed that kaempferitrin may possess antiviral potential against SARS-CoV-2 [76], whilst in this study, it showed moderate antiviral activity against the seasonal influenza A/H1N1 virus, with IC_{50} value of 47.8 μg/mL. In a study conducted by Won-Kyung Cho and his colleagues [81], they reported that isoquercitrin exert antiviral activity against different influenza A strains, namely (A/PR8/34(H1N1))-GFP, A/PR8/34 viruses, and HBPV-VR-32 (H3N2); however, information regarding compound cytotoxicity and inhibitory concentration values were not provided. We found that isoquercitrin is relatively safe on MDCK cells with CC_{50} value of 0.71 mg/mL as compared to the reference drug with poor antiviral potential against the seasonal influenza (H1N1) virus (IC_{50} value of 167 μg/mL). Nevertheless, the wide disparity in IC_{50} values of some tested phytochemicals could be due to a number of factors such as extraction technique, cellular and viral model variations, or antiviral methods used.

Several studies reported the viricidal potentialities of different molecules through the inhibition of the hemagglutinin protein [118–120]. Accordingly, we investigated the abilities of β-sitosterol and β-sitosterol-*O*-glucoside against such protein. Both compounds exhibited perfect binding combined with excellent energy comparing the reference compound. These findings suggest that β-sitosterol and β-sitosterol-*O*-glucoside exert their strong viricidal activities through direct inactivation of the surface hemagglutinin protein, hindering receptor binding and the subsequent viral entry process [7]. The viral neuraminidase (NA) is present on the surface of influenza viruses, allowing the virus to escape from the host cell [121]. Additionally, the interesting transmembrane protein (M2) of the influenza virus functions as a tiny proton channel in the viral envelope that has an essential role following virus endocytosis [7,122]. To understand the inhibitory effects against viral replication, molecular docking studies have been performed for both compounds against NA and M2 proteins and revealed their perfect binding modes as well as their low binding energies. These data confirmed that β-sitosterol and β-sitosterol-*O*-glucoside can affect IAV at different stages during the influenza virus replication cycle.

During the COVID-19 pandemic, several studies have discussed the male-biased mortality in sex-disaggregated data of COVID-19, suggesting that the female sex hormone estrogen is likely to contribute to partially protecting and alleviating disease severity or progression [113]. Similarly, by analyzing the distribution of the differential significance between numbers of influenza cases and deaths within three influenza seasons in Europe, we also found male-biased mortality in sex-disaggregated data of influenza viruses with significant differences towards males during the 2019 influenza season. Interestingly, phytoestrogens, including β-sitosterol, are structurally similar to endogenous estrogens such

as estradiol [123]. This structural similarity may explain the ability of both estrogens to control IAV replication via similar mechanisms. It is worth mentioning that the phytoestrogen β-sitosterol has more potent antiviral activity when compared with the active form of the female endogenous estrogen, but with fewer expected side effects and high biological side benefits [124,125].

5. Conclusions

Conclusively, our study provides a proof-of-principle demonstration that β-sitosterol (Phytosterol) and β-sitosterol-*O*-glucoside (Sitogluside) significantly have high in vitro antiviral potential against avian and human IAVs. Molecular docking studies were performed and suggested that β-sitosterol and β-sitosterol-*O*-glucoside exerted viricidal activities by binding to hemagglutinin protein. The β-sitosterol could also inhibit viral replication via interfering with viral neuraminidase and M2 proteins of IAV. This study also highlighted the possible estrogen-like effect of β-sitosterol due to the structural similarities between the two molecules and proved the anti-influenza activity of estradiol as the most active form of estrogen.

References

1. Naghavi, M.; Abajobir, A.A.; Abbafati, C.; Abbas, K.M.; Abd-Allah, F.; Abera, S.F.; Aboyans, V.; Adetokunboh, O.; Afshin, A.; Agrawal, A. Global, regional, and national age-sex specific mortality for 264 causes of death, 1980–2016: A systematic analysis for the global burden of disease study 2016. *Lancet* **2017**, *390*, 1151–1210. [CrossRef] [PubMed]
2. Rolfes, M.A.; Foppa, I.M.; Garg, S.; Flannery, B.; Brammer, L.; Singleton, J.A.; Burns, E.; Jernigan, D.; Olsen, S.J.; Bresee, J. Annual estimates of the burden of seasonal influenza in the united states: A tool for strengthening influenza surveillance and preparedness. *Influenza Other Respir. Viruses* **2018**, *12*, 132–137. [CrossRef] [PubMed]
3. Martin, L.J.; Im, C.; Dong, H.; Lee, B.E.; Talbot, J.; Meurer, D.P.; Mukhi, S.N.; Drews, S.J.; Yasui, Y. Influenza-like illness-related emergency department visits: Christmas and new year holiday peaks and relationships with laboratory-confirmed respiratory virus detections, edmonton, alberta, 2004–2014. *Influenza Other Respir. Viruses* **2017**, *11*, 33–40. [CrossRef]
4. Kesson, A.M. Respiratory virus infections. *Paediatr. Respir. Rev.* **2007**, *8*, 240–248. [CrossRef] [PubMed]
5. White, D.O.; Brown, L.E. Respiratory viruses. In *Encyclopedia of Virology*; Academic Press: Cambridge, MA, USA, 1999; pp. 1488–1496. [CrossRef]
6. Al-Karmalawy, A.A.; Soltane, R.; Abo Elmaaty, A.; Tantawy, M.A.; Antar, S.A.; Yahya, G.; Chrouda, A.; Pashameah, R.A.; Mustafa, M.; Abu Mraheil, M.; et al. Coronavirus disease (COVID-19) control between drug repurposing and vaccination: A comprehensive overview. *Vaccines* **2021**, *9*, 1317. [CrossRef] [PubMed]
7. Mostafa, A.; Abdelwhab, E.M.; Mettenleiter, T.C.; Pleschka, S. Zoonotic potential of influenza a viruses: A comprehensive overview. *Viruses* **2018**, *10*, 497. [CrossRef] [PubMed]
8. Wright, P.; Neumann, G.; Kawaoka, Y. Orthomyxoviruses. Fields virology. In *Fields Virology*, 5th ed.; Lippincott-Williams & Wilkins: Philadelphia, PA, USA, 2007; Volume 1, pp. 1691–1740.
9. Taubenberger, J.K.; Morens, D.M. The pathology of influenza virus infections. *Annu. Rev. Pathol.* **2008**, *3*, 499–522. [CrossRef] [PubMed]

10. Shahrajabian, M.H.; Sun, W.; Cheng, Q. Product of natural evolution (sars, mers, and SARS-CoV-2); deadly diseases, from sars to SARS-CoV-2. *Hum. Vaccin. Immunother.* **2021**, *17*, 62–83. [CrossRef]

11. Putri, W.C.; Muscatello, D.J.; Stockwell, M.S.; Newall, A.T. Economic burden of seasonal influenza in the united states. *Vaccine* **2018**, *36*, 3960–3966. [CrossRef]

12. Okomo, U.; Idoko, O.T.; Kampmann, B. The burden of viral respiratory infections in young children in low-resource settings. *Lancet Glob. Health* **2020**, *8*, e454–e455. [CrossRef]

13. Iuliano, A.D.; Roguski, K.M.; Chang, H.H.; Muscatello, D.J.; Palekar, R.; Tempia, S.; Cohen, C.; Gran, J.M.; Schanzer, D.; Cowling, B.J. Estimates of global seasonal influenza-associated respiratory mortality: A modelling study. *Lancet* **2018**, *391*, 1285–1300. [CrossRef] [PubMed]

14. Sellers, S.A.; Hagan, R.S.; Hayden, F.G.; Fischer, W.A., 2nd. The hidden burden of influenza: A review of the extra-pulmonary complications of influenza infection. *Influenza Other Respir Viruses* **2017**, *11*, 372–393. [CrossRef] [PubMed]

15. Krammer, F.; Smith, G.J.D.; Fouchier, R.A.M.; Peiris, M.; Kedzierska, K.; Doherty, P.C.; Palese, P.; Shaw, M.L.; Treanor, J.; Webster, R.G.; et al. Influenza. *Nat. Rev. Dis. Prim.* **2018**, *4*, 3. [CrossRef] [PubMed]

16. Barr, J.N.; Fearns, R. Genetic instability of rna viruses. In *Genome Stability*; Academic Press: Cambridge, MA, USA, 2016; pp. 21–35. [CrossRef]

17. Wat, D. The common cold: A review of the literature. *Eur. J. Intern. Med.* **2004**, *15*, 79–88. [CrossRef] [PubMed]

18. Boncristiani, H.F.; Criado, M.F.; Arruda, E. Respiratory viruses. In *Encyclopedia of Microbiology*; Academic Press: Cambridge, MA, USA, 2009; pp. 500–518. [CrossRef]

19. Musarra-Pizzo, M.; Pennisi, R.; Ben-Amor, I.; Mandalari, G.; Sciortino, M.T. Antiviral activity exerted by natural products against human viruses. *Viruses* **2021**, *13*, 828. [CrossRef]

20. Hegazy, A.; Mostafa, I.; Elshaier, Y.A.M.M.; Mahmoud, S.H.; Abo Shama, N.M.; Shehata, M.; Yahya, G.; Nasr, N.F.; El-Halawany, A.M.; Ali, M.A.; et al. Robust antiviral activity of santonica flower extract (artemisia cina) against avian and human influenza a viruses: In vitro and chemoinformatic studies. *ACS Omega* **2022**, *7*, 41212–41223. [CrossRef]

21. Lin, L.T.; Hsu, W.C.; Lin, C.C. Antiviral natural products and herbal medicines. *J. Tradit. Complement. Med.* **2014**, *4*, 24–35. [CrossRef]

22. Li, H.; Sun, J.; Xiao, S.; Zhang, L.; Zhou, D. Triterpenoid-mediated inhibition of virus–host interaction: Is now the time for discovering viral entry/release inhibitors from nature? *J. Med. Chem.* **2020**, *63*, 15371–15388. [CrossRef]

23. Mostafa, A.; Mahmoud, S.H.; Shehata, M.; Müller, C.; Kandeil, A.; El-Shesheny, R.; Nooh, H.Z.; Kayali, G.; Ali, M.A.; Pleschka, S. Pa from a recent h9n2 (g1-like) avian influenza a virus (aiv) strain carrying lysine 367 confers altered replication efficiency and pathogenicity to contemporaneous h5n1 in mammalian systems. *Viruses* **2020**, *12*, 1046. [CrossRef]

24. Petersen, H.; Mostafa, A.; Tantawy, M.A.; Iqbal, A.A.; Hoffmann, D.; Tallam, A.; Selvakumar, B.; Pessler, F.; Beer, M.; Rauten-schlein, S. Ns segment of a 1918 influenza a virus-descendent enhances replication of h1n1pdm09 and virus-induced cellular immune response in mammalian and avian systems. *Front. Microbiol.* **2018**, *9*, 526. [CrossRef]

25. Sarg, T.M.; El-Domiaty, M.M.; Ateya, A.-M.M.; EI-Dahmy, S.I.; EI-Shazly, A.M. Phytochemical investigation of cen-taurea eryn-gioides lam. Growing in egypt. *Alex. J. Pharm. Sci.* **1993**, *7*, 50–54.

26. Hamdan, D.; El-Readi, M.Z.; Tahrani, A.; Herrmann, F.; Kaufmann, D.; Farrag, N.; El-Shazly, A.; Wink, M. Chemical composition and biological activity of citrus jambhiri lush. *Food Chem.* **2011**, *127*, 394–403. [CrossRef] [PubMed]

27. Bosch-Barrera, J.; Martin-Castillo, B.; Buxó, M.; Brunet, J.; Encinar, J.A.; Menendez, J.A. Silibinin and SARS-CoV-2: Dual targeting of host cytokine storm and virus replication machinery for clinical management of COVID-19 patients. *J. Clin. Med.* **2020**, *9*, 1770. [CrossRef] [PubMed]

28. Dai, J.-P.; Wu, L.-Q.; Li, R.; Zhao, X.-F.; Wan, Q.-Y.; Chen, X.-X.; Li, W.-Z.; Wang, G.-F.; Li, K.-S. Identification of 23-(s)-2-amino-3-phenylpropanoyl-silybin as an antiviral agent for influenza a virus infection in vitro and in vivo. *Antimicrob. Agents Chemother.* **2013**, *57*, 4433–4443. [CrossRef]

29. Jin, Z.; Yang, Y.-Z.; Chen, J.-X.; Tang, Y.-Z. Inhibition of pro-inflammatory mediators in raw264. 7 cells by 7-hydroxyflavone and 7, 8-dihydroxyflavone. *J. Pharm. Pharmacol.* **2017**, *69*, 865–874. [CrossRef]

30. Wang, J.; Su, H.; Zhang, T.; Du, J.; Cui, S.; Yang, F.; Jin, Q. Inhibition of enterovirus 71 replication by 7-hydroxyflavone and diisopropyl-flavon7-yl phosphate. *PLoS ONE* **2014**, *9*, e92565. [CrossRef]

31. Lalani, S.; Poh, C.L. Flavonoids as antiviral agents for enterovirus a71 (ev-a71). *Viruses* **2020**, *12*, 184. [CrossRef]

32. Schnitzler, P.; Neuner, A.; Nolkemper, S.; Zundel, C.; Nowack, H.; Sensch, K.H.; Reichling, J. Antiviral activity and mode of action of propolis extracts and selected compounds. *Phytother. Res.* **2010**, *24*, S20–S28. [CrossRef]

33. Le Lee, J.; Loe, M.W.C.; Lee, R.C.H.; Chu, J.J.H. Antiviral activity of pinocembrin against zika virus replication. *Antivir. Res.* **2019**, *167*, 13–24. [CrossRef]

34. González-Búrquez, M.d.J.; González-Díaz, F.R.; García-Tovar, C.G.; Carrillo-Miranda, L.; Soto-Zárate, C.I.; Canales-Martínez, M.M.; Penieres-Carrillo, J.G.; Crúz-Sánchez, T.A.; Fonseca-Coronado, S. Comparison between in vitro antiviral effect of mexican propolis and three commercial flavonoids against canine distemper virus. *Evid. -Based Complement. Altern. Med.* **2018**, *2018*, 7092416. [CrossRef]

35. Guler, H.I.; Tatar, G.; Yildiz, O.; Belduz, A.O.; Kolayli, S. Investigation of potential inhibitor properties of ethanolic propolis extracts against ace-ii receptors for COVID-19 treatment by molecular docking study. *Arch. Microbiol.* **2021**, *203*, 3557–3564. [CrossRef]

36. Alalaiwe, A.; Lin, C.-F.; Hsiao, C.-Y.; Chen, E.-L.; Lin, C.-Y.; Lien, W.-C.; Fang, J.-Y. Development of flavanone and its derivatives as topical agents against psoriasis: The prediction of therapeutic efficiency through skin permeation evaluation and cell-based assay. *Int. J. Pharm.* **2020**, *581*, 119256. [CrossRef] [PubMed]

37. Figueiredo, G.; Coronel, O.; Trabuco, A.; Bazán, D.; Russo, R.; Alvarenga, N.; Aquino, V. Steroidal saponins from the roots of solanum sisymbriifolium lam.(solanaceae) have inhibitory activity against dengue virus and yellow fever virus. *Braz. J. Med. Biol. Res.* **2021**, *54*, e10240. [CrossRef] [PubMed]

38. Desai, T.H.; Joshi, S.V. Anticancer activity of saponin isolated from albizia lebbeck using various in vitro models. *J. Ethnopharmacol.* **2019**, *231*, 494–502. [CrossRef] [PubMed]

39. Pham, H.N.T.; Sakoff, J.A.; Vuong, Q.V.; Bowyer, M.C.; Scarlett, C.J. Phytochemical, antioxidant, anti-proliferative and antimicrobial properties of catharanthus roseus root extract, saponin-enriched and aqueous fractions. *Mol. Biol. Rep.* **2019**, *46*, 3265–3273. [CrossRef]

40. Mair, C.E.; Grienke, U.; Wilhelm, A.; Urban, E.; Zehl, M.; Schmidtke, M.; Rollinger, J.M. Anti-influenza triterpene saponins from the bark of burkea africana. *J. Nat. Prod.* **2018**, *81*, 515–523. [CrossRef]

41. Wang, W.-H.; Chuang, H.-Y.; Chen, C.-H.; Chen, W.-K.; Hwang, J.-J. Lupeol acetate ameliorates collagen-induced arthritis and osteoclastogenesis of mice through improvement of microenvironment. *Biomed. Pharmacother.* **2016**, *79*, 231–240. [CrossRef]

42. Pereira Beserra, F.; Sérgio Gushiken, L.F.; Vieira, A.J.; Augusto Bérgamo, D.; Luísa Bérgamo, P.; Oliveira de Souza, M.; Alberto Hussni, C.; Kiomi Takahira, R.; Henrique Nóbrega, R.; Monteiro Martinez, E.R. From inflammation to cutaneous repair: Topical application of lupeol improves skin wound healing in rats by modulating the cytokine levels, nf-κb, ki-67, growth factor expression, and distribution of collagen fibers. *Int. J. Mol. Sci.* **2020**, *21*, 4952. [CrossRef]

43. Smirnova, I.E.; Kazakova, O.B. Structure–anti-influenza type a activity relationship among a series of nitrogen lupane triterpenoids. *Nat. Prod. Commun.* **2018**, *13*, 1934578X1801301008. [CrossRef]

44. Martínez-Leal, J.; Ponce-García, N.; Escalante-Aburto, A. Recent evidence of the beneficial effects associated with glucuronic acid contained in kombucha beverages. *Curr. Nutr. Rep.* **2020**, *9*, 163–170. [CrossRef]

45. Chen, Y.; Luo, Q.; Li, S.; Li, C.; Liao, S.; Yang, X.; Zhou, R.; Zhu, Y.; Teng, L.; Chen, H. Antiviral activity against porcine epidemic diarrhea virus of pogostemon cablin polysaccharide. *J. Ethnopharmacol.* **2020**, *259*, 113009. [CrossRef] [PubMed]

46. Song, W.; Si, L.; Ji, S.; Wang, H.; Fang, X.-m.; Yu, L.-y.; Li, R.-y.; Liang, L.-n.; Zhou, D.; Ye, M. Uralsaponins m–y, antiviral triterpenoid saponins from the roots of glycyrrhiza uralensis. *J. Nat. Prod.* **2014**, *77*, 1632–1643. [CrossRef] [PubMed]

47. Cheng, D.; Sun, L.; Zou, S.; Chen, J.; Mao, H.; Zhang, Y.; Liao, N.; Zhang, R. Antiviral effects of houttuynia cordata polysaccharide extract on murine norovirus-1 (mnv-1)—A human norovirus surrogate. *Molecules* **2019**, *24*, 1835. [CrossRef] [PubMed]

48. Cui, W.; Huang, J.; Niu, X.; Shang, H.; Sha, Z.; Miao, Y.; Wang, H.; Chen, R.; Wei, K.; Zhu, R. Screening active fractions from pinus massoniana pollen for inhibiting alv-j replication and their structure activity relationship investigation. *Vet. Microbiol.* **2021**, *252*, 108908. [CrossRef] [PubMed]

49. Chun, B.K.; Schinazi, R.F.; Cheng, Y.-C.; Chu, C.K. Synthesis of 2′, 3′-dideoxy-3′-fluoro-l-ribonucleosides as potential antiviral agents from d-sorbitol. *Carbohydr. Res.* **2000**, *328*, 49–59. [CrossRef]

50. Zhang, H.; Saravanan, K.M.; Yang, Y.; Hossain, M.; Li, J.; Ren, X.; Pan, Y.; Wei, Y. Deep learning based drug screening for novel coronavirus 2019-ncov. *Interdiscip. Sci. Comput. Life Sci.* **2020**, *12*, 368–376. [CrossRef]

51. Maiyoa, F.; Moodley, R.; Singh, M. Phytochemistry, cytotoxicity and apoptosis studies of β-sitosterol-3-oglucoside and β-amyrin from prunus africana. *Afr. J. Tradit. Complement. Altern. Med.* **2016**, *13*, 105–112. [CrossRef]

52. Zhou, B.-x.; Li, J.; Liang, X.-l.; Pan, X.-p.; Hao, Y.-b.; Xie, P.-f.; Jiang, H.-m.; Yang, Z.-f.; Zhong, N.-s. B-sitosterol ameliorates influenza a virus-induced proinflammatory response and acute lung injury in mice by disrupting the cross-talk between rig-i and ifn/stat signaling. *Acta Pharmacol. Sin.* **2020**, *41*, 1178–1196. [CrossRef]

53. Chen, C.; Shen, J.-L.; Liang, C.-S.; Sun, Z.-C.; Jiang, H.-F. First discovery of beta-sitosterol as a novel antiviral agent against white spot syndrome virus. *Int. J. Mol. Sci.* **2022**, *23*, 10448. [CrossRef]

54. Khan, S.L.; Siddiqui, F.A. Beta-sitosterol: As immunostimulant, antioxidant and inhibitor of SARS-CoV-2 spike glycoprotein. *Arch. Pharmacol. Ther.* **2020**, *2*, 12–16.

55. Zainab, B.; Ayaz, Z.; Alwahibi, M.S.; Khan, S.; Rizwana, H.; Soliman, D.W.; Alawaad, A.; Abbasi, A.M. In-silico elucidation of moringa oleifera phytochemicals against diabetes mellitus. *Saudi J. Biol. Sci.* **2020**, *27*, 2299–2307. [CrossRef] [PubMed]

56. Behloul, N.; Baha, S.; Guo, Y.; Yang, Z.; Shi, R.; Meng, J. In silico identification of strong binders of the SARS-CoV-2 receptor-binding domain. *Eur. J. Pharmacol.* **2021**, *890*, 173701. [CrossRef] [PubMed]

57. Gao, P.; Huang, X.; Liao, T.; Li, G.; Yu, X.; You, Y.; Huang, Y. Daucosterol induces autophagic-dependent apoptosis in prostate cancer via jnk activation. *Biosci. Trends* **2019**, *13*, 160–167. [CrossRef] [PubMed]

58. Laverdière, I.; Boileau, M.; Neumann, A.L.; Frison, H.; Mitchell, A.; Ng, S.W.; Wang, J.C.; Minden, M.D.; Eppert, K. Leukemic stem cell signatures identify novel therapeutics targeting acute myeloid leukemia. *Blood Cancer J.* **2018**, *8*, 1–16. [CrossRef]

59. Yang, C.-W.; Chang, H.-Y.; Lee, Y.-Z.; Hsu, H.-Y.; Lee, S.-J. The cardenolide ouabain suppresses coronaviral replication via augmenting a na+/k+-atpase-dependent pi3k_pdk1 axis signaling. *Toxicol. Appl. Pharmacol.* **2018**, *356*, 90–97. [CrossRef]

60. Cho, J.; Lee, Y.J.; Kim, J.H.; Kim, S.S.; Choi, B.-S.; Choi, J.-H. Antiviral activity of digoxin and ouabain against SARS-CoV-2 infection and its implication for COVID-19. *Sci. Rep.* **2020**, *10*, 1–8. [CrossRef]

61. Katzen, J.; Hurtado, J.; Lecuona, E.; Sznajder, J.I. B32 viral infection of the airway: The cardioactive glycoside ouabain inhibits influenza a viral replication. *Am. J. Respir. Crit. Care Med.* **2014**, *189*, 1.

62. Fan, H.Y.; Heerklotz, H. Digitonin does not flip across cholesterol-poor membranes. *J. Colloid Interface Sci.* **2017**, *504*, 283–293. [CrossRef]

63. Orczyk, M.; Wojciechowski, K.; Brezesinski, G. Disordering effects of digitonin on phospholipid monolayers. *Langmuir* **2017**, *33*, 3871–3881. [CrossRef]

64. Zhang, J.-W.; Wang, H.; Liu, J.; Ma, L.; Hua, R.-H.; Bu, Z.-G. Generation of a stable gfp-reporter zika virus system for high-throughput screening of zika virus inhibitors. *Virol. Sin.* **2021**, *36*, 476–489. [CrossRef]

65. Inoue, Y.; Hasegawa, S.; Yamada, T.; Date, Y.; Mizutani, H.; Nakata, S.; Matsunaga, K.; Akamatsu, H. Analysis of the effects of hydroquinone and arbutin on the differentiation of melanocytes. *Biol. Pharm. Bull.* **2013**, *36*, 1722–1730. [CrossRef] [PubMed]

66. Baby, K.; Maity, S.; Mehta, C.H.; Suresh, A.; Nayak, U.Y.; Nayak, Y. Targeting SARS-CoV-2 main protease: A computational drug repurposing study. *Arch. Med. Res.* **2021**, *52*, 38–47. [CrossRef] [PubMed]

67. Van Hoof, L.; Totte, J.; Corthout, J.; Pieters, L.; Mertens, F.; Vanden Berghe, D.; Vlietinck, A.; Dommisse, R.; Esmans, E. Plant antiviral agents, vi. Isolation of antiviral phenolic glucosides from populus cultivar beaupre by droplet counter-current chromatography. *J. Nat. Prod.* **1989**, *52*, 875–878. [CrossRef] [PubMed]

68. Ishikawa, T.; Nishigaya, K.; Takami, K.; Uchikoshi, H.; Chen, I.-S.; Tsai, I.-L. Isolation of salicin derivatives from homalium c ochinchinensis and their antiviral activities. *J. Nat. Prod.* **2004**, *67*, 659–663. [CrossRef] [PubMed]

69. Le, N.P.K.; Herz, C.; Gomes, J.V.D.; Förster, N.; Antoniadou, K.; Mittermeier-Kleßinger, V.K.; Mewis, I.; Dawid, C.; Ulrichs, C.; Lamy, E. Comparative anti-inflammatory effects of salix cortex extracts and acetylsalicylic acid in SARS-CoV-2 peptide and lps-activated human in vitro systems. *Int. J. Mol. Sci.* **2021**, *22*, 6766. [CrossRef] [PubMed]

70. Nzuza, S.; Ndwandwe, D.E.; Owira, P.M. Naringin protects against hiv-1 protease inhibitors-induced pancreatic β-cell dysfunction and apoptosis. *Mol. Cell. Endocrinol.* **2016**, *437*, 1–10. [CrossRef]

71. Chen, R.; Qi, Q.-L.; Wang, M.-T.; Li, Q.-Y. Therapeutic potential of naringin: An overview. *Pharm. Biol.* **2016**, *54*, 3203–3210. [CrossRef]

72. Huseen, N.H.A. Docking study of naringin binding with COVID-19 main protease enzyme. *Iraqi J. Pharm. Sci.* **2020**, *29*, 231–238. [CrossRef]

73. Nzuza, S.; Zondi, S.; Owira, P.M. Naringin prevents hiv-1 protease inhibitors-induced metabolic complications in vivo. *PLoS ONE* **2017**, *12*, e0183355. [CrossRef]

74. Fang, S.-H.; Rao, Y.K.; Tzeng, Y.-M. Inhibitory effects of flavonol glycosides from cinnamomum osmophloeum on inflammatory mediators in lps/ifn-γ-activated murine macrophages. *Bioorganic Med. Chem.* **2005**, *13*, 2381–2388. [CrossRef]

75. Choi, J.-G.; Kim, Y.S.; Kim, J.H.; Chung, H.-S. Antiviral activity of ethanol extract of geranii herba and its components against influenza viruses via neuraminidase inhibition. *Sci. Rep.* **2019**, *9*, 1–12. [CrossRef]

76. Singh, R.; Bhardwaj, V.K.; Sharma, J.; Purohit, R.; Kumar, S. In-silico evaluation of bioactive compounds from tea as potential SARS-CoV-2 nonstructural protein 16 inhibitors. *J. Tradit. Complement. Med.* **2022**, *12*, 35–43. [CrossRef] [PubMed]

77. Jorge, A.P.; Horst, H.; de Sousa, E.; Pizzolatti, M.G.; Silva, F.R.M.B. Insulinomimetic effects of kaempferitrin on glycaemia and on 14c-glucose uptake in rat soleus muscle. *Chem. -Biol. Interact.* **2004**, *149*, 89–96. [CrossRef] [PubMed]

78. Huang, X.-L.; He, Y.; Ji, L.-L.; Wang, K.-Y.; Wang, Y.-L.; Chen, D.-F.; Geng, Y.; OuYang, P.; Lai, W.-M. Hepatoprotective potential of isoquercitrin against type 2 diabetes-induced hepatic injury in rats. *Oncotarget* **2017**, *8*, 101545. [CrossRef] [PubMed]

79. Resham, K.; Khare, P.; Bishnoi, M.; Sharma, S.S. Neuroprotective effects of isoquercitrin in diabetic neuropathy via wnt/β-catenin signaling pathway inhibition. *Biofactors* **2020**, *46*, 411–420. [CrossRef]

80. Gao, Z.; Luan, Y.; Yang, P.; Wang, L.; Zhang, H.; Jing, S.; Wang, L.; Wang, T.; Wang, D. Targeting staphylocoagulase with isoquercitrin protects mice from staphylococcus aureus–induced pneumonia. *Appl. Microbiol. Biotechnol.* **2020**, *104*, 3909–3919. [CrossRef]

81. Cho, W.-K.; Yang, H.J.; Ma, J.Y. Lotus (nelumbo nucifera gaertn.) leaf water extracts suppress influenza a viral infection via inhibition of neuraminidase and hemagglutinin. *J. Funct. Foods* **2022**, *91*, 105019. [CrossRef]

82. Ling, L.-j.; Lu, Y.; Zhang, Y.-y.; Zhu, H.-y.; Tu, P.; Li, H.; Chen, D.-f. Flavonoids from houttuynia cordata attenuate h1n1-induced acute lung injury in mice via inhibition of influenza virus and toll-like receptor signalling. *Phytomedicine* **2020**, *67*, 153150. [CrossRef]

83. Semple, S.J.; Pyke, S.M.; Reynolds, G.D.; Flower, R.L. In vitro antiviral activity of the anthraquinone chrysophanic acid against poliovirus. *Antivir. Res.* **2001**, *49*, 169–178. [CrossRef]

84. Narkhede, R.R.; Pise, A.V.; Cheke, R.S.; Shinde, S.D. Recognition of natural products as potential inhibitors of COVID-19 main protease (mpro): In-silico evidences. *Nat. Prod. Bioprospecting* **2020**, *10*, 297–306. [CrossRef]

85. Dong, X.; Zeng, Y.; Liu, Y.; You, L.; Yin, X.; Fu, J.; Ni, J. Aloe-emodin: A review of its pharmacology, toxicity, and pharmacokinetics. *Phytother. Res.* **2020**, *34*, 270–281. [CrossRef] [PubMed]

86. Ho, T.-Y.; Wu, S.-L.; Chen, J.-C.; Li, C.-C.; Hsiang, C.-Y. Emodin blocks the sars coronavirus spike protein and angiotensin-converting enzyme 2 interaction. *Antivir. Res.* **2007**, *74*, 92–101. [CrossRef] [PubMed]

87. Adhikari, B.; Marasini, B.P.; Rayamajhee, B.; Bhattarai, B.R.; Lamichhane, G.; Khadayat, K.; Adhikari, A.; Khanal, S.; Parajuli, N. Potential roles of medicinal plants for the treatment of viral diseases focusing on covid-19: A review. *Phytother. Res.* **2021**, *35*, 1298–1312. [CrossRef] [PubMed]

88. Robson, B. COVID-19 coronavirus spike protein analysis for synthetic vaccines, a peptidomimetic antagonist, and therapeutic drugs, and analysis of a proposed achilles' heel conserved region to minimize probability of escape mutations and drug resistance. *Comput. Biol. Med.* **2020**, *121*, 103749. [CrossRef] [PubMed]

89. Cheng, C.; Dong, W. Aloe-emodin induces endoplasmic reticulum stress-dependent apoptosis in colorectal cancer cells. *Med. Sci. Monit. Int. Med. J. Exp. Clin. Res.* **2018**, *24*, 6331. [CrossRef]

90. Li, S.-W.; Yang, T.-C.; Lai, C.-C.; Huang, S.-H.; Liao, J.-M.; Wan, L.; Lin, Y.-J.; Lin, C.-W. Antiviral activity of aloe-emodin against influenza a virus via galectin-3 up-regulation. *Eur. J. Pharmacol.* **2014**, *738*, 125–132. [CrossRef]

91. Liu, Z.; Ma, N.; Zhong, Y.; Yang, Z.-q. Antiviral effect of emodin from rheum palmatum against coxsakievirus b5 and human respiratory syncytial virus in vitro. *J. Huazhong Univ. Sci. Technol. [Med. Sci.]* **2015**, *35*, 916–922. [CrossRef]

92. Hsu, C.-L.; Yen, G.-C. Effects of flavonoids and phenolic acids on the inhibition of adipogenesis in 3t3-l1 adipocytes. *J. Agric. Food Chem.* **2007**, *55*, 8404–8410. [CrossRef]

93. Santos, P.M.; Vieira, A.J. Antioxidising activity of cinnamic acid derivatives against oxidative stress induced by oxidising radicals. *J. Phys. Org. Chem.* **2013**, *26*, 432–439. [CrossRef]

94. Sharma, P.; Singh, R. Efficacy of trans-2-hydroxycinnamic acid against trichlorfon-induced oxidative stress in wistar rats. *Toxicol. Int.* **2012**, *19*, 295.

95. Enkhtaivan, G.; John, K.M.; Ayyanar, M.; Sekar, T.; Jin, K.-J.; Kim, D.H. Anti-influenza (h1n1) potential of leaf and stem bark extracts of selected medicinal plants of south india. *Saudi J. Biol. Sci.* **2015**, *22*, 532–538. [CrossRef] [PubMed]

96. Yadav, R.; Saini, D.; Yadav, D. Synthesis and evaluation of vanillin derivatives as antimicrobial agents. *Turk. J. Pharm. Sci.* **2018**, *15*, 57. [CrossRef] [PubMed]

97. Zhang, J.; Zhao, L.; Zhu, C.; Wu, Z.; Zhang, G.; Gan, X.; Liu, D.; Pan, J.; Hu, D.; Song, B. Facile synthesis of novel vanillin derivatives incorporating a bis (2-hydroxyethyl) dithhioacetal moiety as antiviral agents. *J. Agric. Food Chem.* **2017**, *65*, 4582–4588. [CrossRef] [PubMed]

98. Dhanalakshmi, C.; Janakiraman, U.; Manivasagam, T.; Justin Thenmozhi, A.; Essa, M.M.; Kalandar, A.; Khan, M.A.S.; Guillemin, G.J. Vanillin attenuated behavioural impairments, neurochemical deficts, oxidative stress and apoptosis against rotenone induced rat model of parkinson's disease. *Neurochem. Res.* **2016**, *41*, 1899–1910. [CrossRef]

99. Hariono, M.; Abdullah, N.; Damodaran, K.; Kamarulzaman, E.E.; Mohamed, N.; Hassan, S.S.; Shamsuddin, S.; Wahab, H.A. Potential new h1n1 neuraminidase inhibitors from ferulic acid and vanillin: Molecular modelling, synthesis and in vitro assay. *Sci. Rep.* **2016**, *6*, 1–10. [CrossRef]

100. Law, W.Y.; Asaruddin, M.R.; Bhawani, S.A.; Mohamad, S. Pharmacophore modelling of vanillin derivatives, favipiravir, chloroquine, hydroxychloroquine, monolaurin and tetrodotoxin as mpro inhibitors of severe acute respiratory syndrome coronavirus-2 (SARS-CoV-2). *BMC Res. Notes* **2020**, *13*, 1–8. [CrossRef]

101. Mondal, D. Zanamivir ☆. In *Reference Module in Biomedical Sciences*; Elsevier: Amsterdam, The Netherlands, 2016.

102. Mahmoud, A.; Mostafa, A.; Al-Karmalawy, A.A.; Zidan, A.; Abulkhair, H.S.; Mahmoud, S.H.; Shehata, M.; Elhefnawi, M.M.; Ali, M.A. Telaprevir is a potential drug for repurposing against SARS-CoV-2: Computational and in vitro studies. *Heliyon* **2021**, *7*, e07962. [CrossRef]

103. Mostafa, A.; Kandeil, A.; AMM Elshaier, Y.; Kutkat, O.; Moatasim, Y.; Rashad, A.A.; Shehata, M.; Gomaa, M.R.; Mahrous, N.; Mahmoud, S.H. Fda-approved drugs with potent in vitro antiviral activity against severe acute respiratory syndrome coronavirus 2. *Pharmaceuticals* **2020**, *13*, 443. [CrossRef]

104. EUROSTAT. Causes of Death—Standardised Death Rate by Nuts 2 Region of Residence. Available online: https://ec.europa.eu/eurostat/databrowser/view/hlth_cd_asdr2/default/table?lang=en (accessed on 14 January 2023).

105. Metsalu, T.; Vilo, J. Clustvis: A web tool for visualizing clustering of multivariate data using principal component analysis and heatmap. *Nucleic Acids Res.* **2015**, *43*, W566–W570. [CrossRef]

106. Alesawy, M.S.; Abdallah, A.E.; Taghour, M.S.; Elkaeed, E.B.H. Eissa, I.; Metwaly, A.M. In silico studies of some isoflavonoids as potential candidates against COVID-19 targeting human ace2 (hace2) and viral main protease (mpro). *Molecules* **2021**, *26*, 2806. [CrossRef]

107. Hagras, M.; El Deeb, M.A.; Elzahabi, H.S.; Elkaeed, E.B.; Mehany, A.B.; Eissa, I.H. Discovery of new quinolines as potent colchicine binding site inhibitors: Design, synthesis, docking studies, and anti-proliferative evaluation. *J. Enzym. Inhib. Med. Chem.* **2021**, *36*, 640–658. [CrossRef] [PubMed]

108. Alanazi, M.M.; Mahdy, H.A.; Alsaif, N.A.; Obaidullah, A.J.; Alkahtani, H.M.; Al-Mehizia, A.A.; Alsubaie, S.M.; Dahab, M.A.; Eissa, I.H. New bis ([1,2,4] triazolo)[4,3-a: 3′,4′-c] quinoxaline derivatives as vegfr-2 inhibitors and apoptosis inducers: Design, synthesis, in silico studies, and anticancer evaluation. *Bioorganic Chem.* **2021**, *112*, 104949. [CrossRef] [PubMed]

109. Li, Y.; Han, L.; Liu, Z.; Wang, R. Comparative assessment of scoring functions on an updated benchmark: 2. Evaluation methods and general results. *J. Chem. Inf. Model.* **2014**, *54*, 1717–1736. [CrossRef]

110. Pawar, S.S.; Rohane, S.H. Review on discovery studio: An important tool for molecular docking. *Asian J. Res. Chem* **2021**, *14*, 86–88. [CrossRef]

111. Yousef, R.G.; Sakr, H.M.; Eissa, I.H.; Mehany, A.B.; Metwaly, A.M.; Elhendawy, M.A.; Radwan, M.M.; ElSohly, M.A.; Abulkhair, H.S.; El-Adl, K. New quinoxaline-2 (1 h)-ones as potential vegfr-2 inhibitors: Design, synthesis, molecular docking, admet profile and anti-proliferative evaluations. *New J. Chem.* **2021**, *45*, 16949–16964. [CrossRef]

112. Alesawy, M.S.; Elkaeed, E.B.; Alsfouk, A.A.; Metwaly, A.M.; Eissa, I.H. In silico screening of semi-synthesized compounds as potential inhibitors for SARS-CoV-2 papain-like protease: Pharmacophoric features, molecular docking, admet, toxicity and dft studies. *Molecules* **2021**, *26*, 6593. [CrossRef]

113. Alwani, M.; Yassin, A.; Al-Zoubi, R.M.; Aboumarzouk, O.M.; Nettleship, J.; Kelly, D.; Al-Qudimat, A.R.; Shabsigh, R. Sex-based differences in severity and mortality in COVID-19. *Rev. Med. Virol.* **2021**, *31*, e2223. [CrossRef]

114. Owen, L.; Laird, K.; Shivkumar, M. Antiviral plant-derived natural products to combat rna viruses: Targets throughout the viral life cycle. *Lett. Appl. Microbiol.* **2022**, *75*, 476–499. [CrossRef]

115. Barbieri, R.; Coppo, E.; Marchese, A.; Daglia, M.; Sobarzo-Sánchez, E.; Nabavi, S.F.; Nabavi, S.M. Phytochemicals for human disease: An update on plant-derived compounds antibacterial activity. *Microbiol. Res.* **2017**, *196*, 44–68. [CrossRef]

116. Newman, D.J.; Cragg, G.M. Natural products as sources of new drugs over the nearly four decades from 01/1981 to 09/2019. *J. Nat. Prod.* **2020**, *83*, 770–803. [CrossRef]

117. Gao, Y.; Tai, W.; Wang, N.; Li, X.; Jiang, S.; Debnath, A.K.; Du, L.; Chen, S. Identification of novel natural products as effective and broad-spectrum anti-zika virus inhibitors. *Viruses* **2019**, *11*, 1019. [CrossRef] [PubMed]

118. Shen, X.; Zhu, Z.; Ding, Y.; Wu, W.; Yang, J.; Liu, S. An oligothiophene compound neutralized influenza a viruses by interfering with hemagglutinin. *Biochim. Et Biophys. Acta (BBA) -Biomembr.* **2018**, *1860*, 784–791. [CrossRef] [PubMed]

119. Luganini, A.; Terlizzi, M.E.; Catucci, G.; Gilardi, G.; Maffei, M.E.; Gribaudo, G. The cranberry extract oximacro®exerts in vitro virucidal activity against influenza virus by interfering with hemagglutinin. *Front. Microbiol.* **2018**, *9*, 1826. [CrossRef] [PubMed]

120. Makau, J.N.; Watanabe, K.; Kobayashi, N. Anti-influenza activity of alchemilla mollis extract: Possible virucidal activity against influenza virus particles. *Drug Discov. Ther.* **2013**, *7*, 189–195. [CrossRef]

121. McAuley, J.L.; Gilbertson, B.P.; Trifkovic, S.; Brown, L.E.; McKimm-Breschkin, J.L. Influenza virus neuraminidase structure and functions. *Front. Microbiol.* **2019**, *10*, 39. [CrossRef]

122. Lamb, R.A.; Zebedee, S.L.; Richardson, C.D. Influenza virus m2 protein is an integral membrane protein expressed on the infected-cell surface. *Cell* **1985**, *40*, 627–633. [CrossRef] [PubMed]

123. Brown, A.C.; Stevenson, L.M.; Leonard, H.M.; Nieves-Puigdoller, K.; Clotfelter, E.D. Phytoestrogens β-sitosterol and genistein have limited effects on reproductive endpoints in a female fish, betta splendens. *BioMed Res. Int.* **2014**, *2014*, 681396. [CrossRef]

124. Ju, Y.H.; Clausen, L.M.; Allred, K.F.; Almada, A.L.; Helferich, W.G. B-sitosterol, β-sitosterol glucoside, and a mixture of β-sitosterol and β-sitosterol glucoside modulate the growth of estrogen-responsive breast cancer cells in vitro and in ovariectomized athymic mice. *J. Nutr.* **2004**, *134*, 1145–1151. [CrossRef]

125. Pandey, J.; Dev, K.; Chattopadhyay, S.; Kadan, S.; Sharma, T.; Maurya, R.; Sanyal, S.; Siddiqi, M.I.; Zaid, H.; Tamrakar, A.K. Beta-sitosterol-d-glucopyranoside mimics estrogenic properties and stimulates glucose utilization in skeletal muscle cells. *Molecules* **2021**, *26*, 3129. [CrossRef]